Astronomy & Astrophysics

New massive members of Cygnus OB2

S. R. Berlanas[1,2], A. Herrero[1,2], F. Comerón[3], A. Pasquali[4], C. Bertelli Motta[4], and A. Sota[5]

[1] Instituto de Astrofísica de Canarias, 38200 La Laguna, Tenerife, Spain
   e-mail: srberlan@iac.es
[2] Departamento de Astrofísica, Universidad de La Laguna, 38205 La Laguna, Tenerife, Spain
[3] ESO, Karl-Schwarzschild-Strasse 2, 85748 Garching bei München, Germany
[4] Astronomisches Rechen-Institut, Zentrum für Astronomie der Universität Heidelberg, Mönchhofstr 12-14, 69120 Heidelberg, Germany
[5] Instituto de Astrofísica de Andalucía-CSIC, 18008 Granada, Spain

ABSTRACT

Context. The Cygnus complex is one of the most powerful star forming regions at a close distance from the Sun (~1.4 kpc). Its richest OB association Cygnus OB2 is known to harbor many tens of O-type stars and hundreds of B-type stars, providing a large homogeneous population of OB stars that can be analyzed. Many studies of its massive population have been developed in the last decades, although the total number of OB stars is still incomplete.

Aims. Our aim is to increase the sample of O and B members of Cygnus OB2 and its surroundings by spectroscopically classifying 61 candidates as possible OB-type members of Cygnus OB2, using new intermediate resolution spectroscopy.

Methods. We have obtained intermediate resolution (R ~ 5000) spectra for all of the OB-type candidates between 2013 and 2017. We thus performed a spectral classification of the sample using HeI-II and metal lines rates, as well as the Marxist Ghost Buster (MGB) software for O-type stars and the IACOB standards catalog for B-type stars.

Results. From the whole sample of 61 candidates, we have classified 42 stars as new massive OB-type stars, earlier than B3, in Cygnus OB2 and surroundings, including 11 O-type stars. The other candidates are discarded as they display later spectral types inconsistent with membership in the association. We have also obtained visual extinctions for all the new confirmed massive OB members, placing them in a Hertzsprung-Russell Diagram using calibrations for $T_{\rm eff}$ and luminosity. Finally, we have studied the age and extinction distribution of our sample within the region.

Conclusions. We have obtained new blue intermediate-resolution spectra suitable for spectral classification of 61 OB candidates in Cygnus OB2 and surroundings. The confirmation of 42 new OB massive stars (earlier than B3) in the region allows us to increase the young massive population known in the field. We have also confirmed the correlation between age and Galactic longitude previously found in the region. We conclude that many O and early B stars at $B > 16$ mag are still undiscovered in Cygnus.

Key words. stars: early-type – stars: massive – open clusters and associations: individual: Cygnus OB2 – Hertzsprung-Russell and C-M diagrams – Galaxy: stellar content

1. Introduction

The Cygnus region is the most powerful nearby stellar complex, conspicuous at all wavelengths and very young, with several rich OB associations, numerous young open clusters and tens of compact H II and star formation regions in the field. Hosting the largest number of nearby massive stars and an intense star forming activity (Reipurth & Schneider 2008), it provides an updated view of the high-mass stellar population in one of the largest groups of young stars in our Galaxy. It is an ideal place to study the process of massive star formation and evolution, individually and in stellar groups, and their interaction with the surroundings.

Its association Cygnus OB2 (d ~ 1.4 kpc; Rygl et al. 2012) has received a lot of attention and has been studied at all wavelengths with different spatial coverage since it hosts a high number of early spectral type stars (Walborn et al. 2002). First studies were carried out by Morgan et al. (1954), Schulte (1956, 1958) and Reddish (1968), but it was Massey & Thompson (1991) who developed an extensive survey of the massive population in the association, identifying 120 possible massive star members, 70 of which were classified as OB stars (42 O-type

stars). Knödlseder (2000) proposed that this number should be much larger, around 100 O-type stars. In the last few decades, many other studies were carried out in the region updating continually this number (Comerón et al. 2002, 2008; Hanson 2003; Kiminki et al. 2007; Negueruela et al. 2008; Comerón & Pasquali 2012). These surveys have allowed the global study of the massive population in the region, using photometry to place the stars in a Hertzsprung-Russell diagram (HRD) from which the star formation history and mass function of the association were assessed (Wright et al. 2015). In spite of the many photometric and spectroscopic surveys carried out in the region, only a small homogeneous group of early type stars have been spectroscopically analyzed (Herrero et al. 1999, 2002; Negueruela et al. 2008), and few stars have been observed in the UV range (Herrero et al. 2001). There is still a large number of stars that should be explored. The optical extinction of the region is high ($A_{\rm V}$ = 4.0–7.0 mag; Wright et al. 2015), but not so much as to prevent obtaining spectra of its most massive stars for a rough spectral classification. Therefore, new spectroscopy to search for previously undiscovered massive stars is mandatory to complete the last census of massive O and B-type stars in the association.

Table 1. Telescopes, instruments and settings used in this work.

Instrument and grating	Telescope	Resol.	Date	Stars
ISIS – 600B	ORM-WHT	2500	Oct. 2013	1
WYFFOS – H2400B	ORM-WHT	5000	Jul. 2014	7
ISIS – H2400	ORM-WHT	7500	Jul. 2015	2
OSIRIS – R2500U/V	ORM-GTC	2500	May 2016	2
IDS – R1200B	ORM-INT	5000	Jul. 2016	47
ISIS – R1200B	ORM-WHT	5000	Apr. 2017	2

One of the most complete spectroscopic surveys in the Cygnus region was developed by Comerón & Pasquali (2012). They performed spectral classification of a magnitude-limited sample ($B \leq 16$ mag and $Ks < 9$ mag) selected with a homogeneous photometric criterion over a large area that includes Cygnus OB2 and its surroundings, providing a large sample of known and new OB stars, as well as a list of 61 OB candidates for which no spectral data is available and that are pending spectroscopic confirmation.

The main goal of this work is to complete the spectral classification of this latter sample, aiming a later determination of the stellar parameters. Thus, we have obtained intermediate-resolution spectra of all the list candidates, in order to confirm or reject them as true massive OB-type stars. In Sect. 2 we present the observations. In Sect. 3 we describe the spectral classification criteria used in this work, and in Sect. 4 visual extinctions and stellar parameters derived for the new OB-type members. The results are discussed in Sect. 5 where we show the HRD of the region and the age distribution found across Galactic longitude. Finally, we summarize our conclusions in Sect. 6.

2. Observations and data reduction

The study developed by Comerón & Pasquali (2012) produced a sample of O and early B stars (in a $6° \times 4°$ region centered on Galactic coordinates $l = 79.8°$ and $b = +0.8°$ of Cygnus OB2) which were identified using two homogeneous reddening-free criteria

$$Q_{BJK} = 0.196(B - J) - 0.981(J - K) - 0.098 > 0 \quad (1)$$

$$Q_{JHK} = 0.447(J - H) - 0.894(H - K) - 0.089 < 0 \quad (2)$$

which allowed them to classify 60 new OB stars and produce a list of 61 candidates pending spectroscopic data. They used *BJHK* photometry tabulated in the USNO-B (Zacharias et al. 2010, 2004) and 2MASS all-sky (Skrutskie et al. 2006) catalogs setting limiting magnitudes of $B \leq 16$ mag and $Ks < 9.0$ mag. By combining these two magnitude cuts with the $(B - K)$ colors of OB stars, Comerón & Pasquali (2012) set up a selection method sensitive to main-sequence stars earlier than B1 and obscured by $A_V < 6.7$ mag.

We have obtained new spectra for all the proposed OB candidates, whose location is shown in Fig. 1. The sample has been observed in five different runs between 2013 and 2017. For an accurate spectral classification of OB-type stars we need blue spectra (4000–5000 Å) where the diagnostic He I-II and metal lines are located.

The bulk of stars were observed in July 2016, obtaining spectra of 47 candidates. We have chosen the R1200B grating of IDS (EEV10) on the *Isaac Newton* Telescope (INT) in
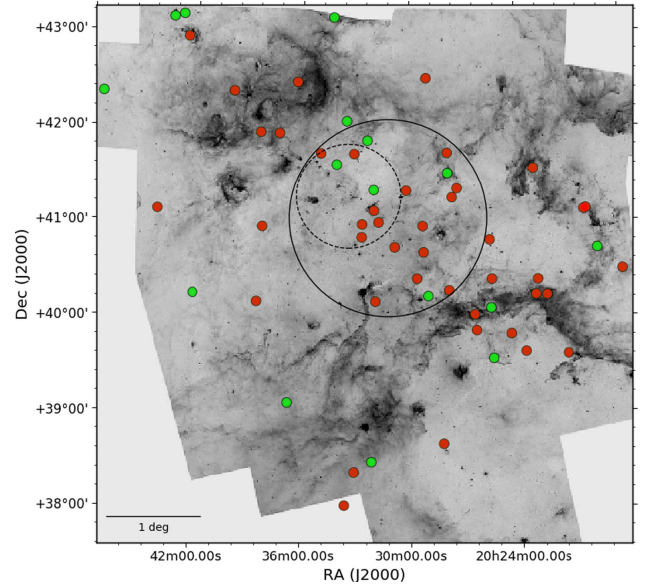
Fig. 1. Inverse *Spitzer* 8 μm image of the Cygnus region showing the location of the 61 OB candidates. The 42 confirmed massive OB-type stars earlier than B3 are indicated with red dots. The remaining stars are late B and foreground A-F-G stars which are indicated with green dots. The solid line circle delimits the 1 deg radius area of Cygnus OB2 adopted by Comerón & Pasquali (2012). For reference, the dash-dotted line circle shows the area considered by Wright et al. (2015).

La Palma, which provides a resolution of ~5000 at 4500 Å. The remaining stars were observed in different runs between 2013 and 2017, at the *William Herschel* Telescope (WHT) using the AF2/WYFFOS and ISIS instruments, and at the Gran Telescopio CANARIAS (GTC) using the OSIRIS instrument. Out of the whole sample, three of the stars (J20301097+4120088, J20315433+4010067, J20345785+4143543) belong to the Galactic O-Star Spectroscopic Survey (GOSSS) catalog (Maíz Apellániz et al. 2016).

The information on the different runs carried out in this work is shown in Table 1. The final spectra were reduced using the IRAF procedures, with standard routines for bias and flat-field subtraction and also for the wavelength calibration.

3. Spectral classification

The accuracy of the spectral classification depends on the effects of spectral resolution as well as the signal-to-noise ratio (S/N). The main diagnostic method for O-type stars is the comparison of He II 4542/He I 4471 ratio (Sota et al. 2011). These lines are similar for a O7 type star. For later O types the relative strengths of He II 4542/He I 4387 and He II 4200/He I 4144 are normally used, and represent the main criteria for types O8-B0. Spectral types earlier than O8 were classified using the criteria described by Gray & Corbally (2009). The presence of metal lines in different ionization stage, such as Si III or Mg II, indicates early B-type stars. The relative strength of HeII 4471/MgII 4481 is a useful indicator for B1-late B stars. As secondary indicators we used the criteria described by Gray & Corbally (2009), which were also used to classify stars of spectral types A, F and G.

Regarding the luminosity class, the criteria used for early O-type stars were introduced by Walborn (1971, 1973), taking into account the emission effects in the He II 4686 line and N III 4634-4640-4642. For late O-type stars, we have used the criteria described by Sota et al. (2011) and for B-type stars the

Table 2. Basic data of the confirmed massive new members (earlier than B3).

Object	RA (hhmmss)	Dec (° ′ ″)	Region	B	Ks	J	SpT	Binary star
J20423509+4256364	20 42 35.08	+42 56 36.43	c	14.480	8.304	9.211	O6IIIz	
J20371773+4156316	20 37 17.73	+41 56 31.57	c	15.760	8.041	9.071	O7V	
J20345785+4143543	20 34 57.84	+41 43 54.25	a	15.430	7.417	8.447	O7:Ib	
J20293563+4024315	20 29 35.63	+40 24 31.45	b	12.468	8.268	8.831	O8IIIz	
J20222481+4013426	20 22 24.81	+40 13 42.55	c	13.620	8.410	9.034	O8II	
J20261976+3951425	20 26 19.75	+39 51 42.46	c	15.600	8.348	9.351	O8.5IV	
J20275292+4144067	20 27 52.92	+41 44 06.65	b	13.330	7.277	8.144	O9.5II	
J20262484+4001413	20 26 24.84	+40 01 41.25	c	13.290	8.330	9.021	O9.2III	
J20291617+4057372	20 29 16.17	+40 57 37.19	b	15.030	7.899	8.855	O9.7III	
J20382173+4157069	20 38 21.72	+41 57 06.89	c	15.810	7.682	8.760	O9.7II	
J20181090+4029063	20 18 10.89	+40 29 06.29	c	14.940	8.399	9.343	O9.7Ib	yes*
J20273787+4115468	20 27 37.87	+41 15 46.79	b	14.570	8.263	9.146	B0II	
J20301097+4120088	20 30 10.97	+41 20 08.82	b	15.690	8.882	9.855	B0:II:	
J20323968+4050418	20 32 39.68	+40 50 41.83	a	14.410	8.913	9.631	B0II	
J20395358+4222506	20 39 53.58	+42 22 50.62	c	15.890	5.822	7.345	B0I	yes*
J20281176+3840227	20 28 11.75	+38 40 22.73	c	11.805	7.944	8.349	B0Ib	
J20323882+4058469	20 32 38.82	+40 58 46.85	a	15.430	8.821	9.701	B0Ib	
J20225451+4023314	20 22 54.50	+40 23 31.39	c	13.107	8.601	9.175	B0Iab	
J20253320+4048444	20 25 33.19	+40 48 44.38	c	13.112	7.648	8.340	B0Iab	
J20272099+4121262	20 27 20.99	+41 21 26.15	b	13.830	8.730	9.448	B0.5V	yes
HDE 229258	20 24 25.51	+39 49 28.30	c	10.235	8.689	8.833	B0.7V	
J20330526+4143367	20 33 05.26	+41 43 36.74	a	13.940	8.634	9.286	B0.5III	
J20361806+4228483	20 36 18.06	+42 28 48.30	c	15.650	8.855	9.814	B0.7III	
J20233816+3938118	20 23 38.16	+39 38 11.84	c	11.293	8.731	8.996	B0.7Ib	
HD 228973	20 20 07.35	+41 07 46.72	c	10.34	7.684	7.922	B1V	yes
J20201435+4107155	20 20 14.34	+41 07 15.45	c	12.412	8.240	8.627	B1V	
J20230290+4133466	20 23 02.90	+41 33 46.59	c	14.780	7.809	8.762	B1V	
BD+404193	20 29 13.55	+40 41 03.38	b	10.412	8.812	8.945	B1V	
BD+404208	20 30 49.97	+40 44 18.53	b	10.654	8.664	8.869	B1V	
J20314341+4100021	20 31 43.40	+41 00 02.07	a	15.940	8.957	9.885	B1V	yes*
J20315898+4107314	20 31 58.98	+41 07 31.41	a	15.490	8.832	9.773	B1V	yes*
J20330453+3822269	20 33 04.53	+38 22 26.91	c	11.383	8.790	9.021	B1V	
J20230183+4014029	20 23 01.83	+40 14 02.90	c	13.465	8.060	8.579	B1III	
J20274925+4017004	20 27 49.25	+40 17 00.42	b	13.460	8.104	8.713	B1III	
J20315433+4010067	20 31 54.33	+40 10 06.71	b	15.990	8.884	9.742	B1III	
J20382889+4009566	20 38 28.88	+40 09 56.63	c	9.996	8.816	8.896	B1III	
J20440752+4107342	20 44 07.51	+41 07 34.18	c	15.470	8.703	9.562	B1III	
LSII+3797	20 33 35.52	+38 01 36.73	c	11.838	5.900	6.691	B1Ia	yes*
J20211924+3936230	20 21 19.24	+39 36 22.98	c	12.732	7.886	8.488	B1Ib	yes*
BD+394179	20 25 27.28	+40 24 00.15	c	11.066	6.667	7.210	B1Ib	
J20290247+4231159	20 29 02.46	+42 31 15.91	c	13.330	8.426	9.090	B1Ib	yes*
J20381289+4057169	20 38 12.88	+40 57 16.86	c	12.870	8.675	9.183	B2V	

Notes. B magnitudes from the USNO-B catalog. Ks and J magnitudes from 2MASS catalog. Region a indicates the 1 deg. circular area centered on Cyg OB2#8 trapezium adopted by Wright et al. (2015) for the Cygnus OB2 association. Region b indicates the 1 deg. radius area adopted by Comerón & Pasquali (2012) for the same Cygnus OB2 association. Region c indicates the surrounding area outside the 1 deg. radius adopted by Comerón & Pasquali (2012). For binary stars asterisks indicate possible SB2 stars, whose spectral types are refered to the primary component.

criteria described by Gray & Corbally (2009) and the Balmer lines width.

Although the classification for O-type stars was based on the described He and metal lines diagnostic criteria, we have also used for O-type stars the Marxist Ghost Buster (MGB) code developed by Maíz Apellániz et al. (2012) in order to obtain a more accurate result. This tool compares the observed spectra with a grid of O standards (in this work the GOSSS library), allowing us to vary spectral type, luminosity class, velocity and resolution until obtaining a best match. Furthermore,

for B-type stars we have used a sample of IACOB standards (Simón-Díaz et al. 2015) to improve their classification.

4. New confirmed OB type stars

The observed spectra have high enough S/N and resolution for a spectral classification of the stars. All the candidate spectra are plotted in Fig. B.1 where the main diagnostic lines used are also indicated.

Table 3. Candidates classified as late B and A-F-G type stars.

Object	RA (hhmmss)	Dec (° ′ ″)
late B-type stars		
CCDMJ20323+4152AB	20 32 20.81	+41 52 00.78
BD+423785a	20 34 15.39	+43 09 35.28
A-type stars		
J20252497+3934030	20 25 24.96	+39 34 03.02
J20285874+4013302	20 28 58.74	+40 13 30.22
J20315984+4120354	20 31 59.84	+41 20 35.41
J20320734+3828586	20 32 07.34	+38 28 58.62
BD+413801	20 33 30.39	+42 04 17.35
J20364336+3906145	20 36 43.36	+39 06 14.53
CCDM J20429+4311AB	20 42 54.24	+43 10 38.71
F-type stars		
J20193232+4042447	20 19 32.32	+40 42 44.72
J20253116+4005508	20 25 31.16	+40 05 50.82
J20275204+4131200	20 27 52.03	+41 31 19.98
CCDM J20420+4015	20 42 01.18	+40 14 42.70
J20500396+4300118	20 50 03.96	+43 00 11.76
J20504551+421012.6	20 50 45.51	+42 10 12.64
G-type stars		
J20300022+4337553	20 30 00.21	+43 37 55.29
J20340430+4136507	20 34 04.29	+41 36 50.67
J20432737+4308525	20 43 27.37	+43 08 52.47
J20472235+4220523	20 47 22.34	+42 20 52.30

Fig. 2. Example of SB2 detection: HeI lines in star HD 228973.

Fig. 3. $(B - K)$, B diagram of the confirmed O-type stars in Cygnus OB2 within the 1 deg. radius area adopted by Comerón & Pasquali (2012). Blue dots indicate stars previously known, and red dots represent the new ones confirmed in this work. The upper left vertical line shows the position of the unreddened main sequence based on intrinsic magnitudes from Martins & Plez (2006) at a distance modulus $DM = 10.8$ mag. The dash-dotted lines represent the locus expected for different spectral type stars using the reddening law of Wright et al. (2015) with $R_V = 2.91$. The solid line marks the limits imposed by the selection criteria at magnitudes $B \leq 16$ mag, $Ks < 9$ mag. Vertical dotted lines indicate $(B - K)$ color bins.

Out of the 61 candidates 42 are OB type stars, earlier than B3, including 11 O-type stars. Two more are late B-type stars. The location of these new confirmed OB stars is shown in Fig. 1 while their names, coordinates, magnitudes and the derived spectral classification are listed in Table 2. We have also included the region in which they are located: (a) the Cygnus OB2 area considered by Wright et al. (2015) which is the youngest core of Cyg OB2 at present; (b) the Cygnus OB2 area considered by Comerón & Pasquali (2012) which is the extended Cyg OB2 area containing older stars, on average, and (c) the surrounding area which includes part of the Cygnus OB9 association and field population. The remaining observed stars are late B and foreground A-F-G stars, which are globally listed in Table 3. The selection criteria success rate obtained by Comerón & Pasquali (2012) along with the number of the confirmed OB type obtained in this work (72%), support the success at identifying reddened massive OB stars with this method.

We have also detected nine possible or confirmed SB2 binaries in the sample of new OB stars (see Table 2). In some cases, indicated with asterisks, we can only suggest possible binary nature mainly due to noisy spectra. This number represents a 21% of our massive OB sample. We assign to these stars the spectral classification of their primary component. An example is shown in Fig. 2. Sana & Evans (2011) found that at least $45 - 55\%$ of the O star population in clusters and OB associations is comprized of spectroscopic binaries, which indicates that it is highly likely that more binaries are undetected in our sample.

4.1. Extinction

We used the $(J - Ks)$ colors and the recent extinction law derived by Wright et al. (2015) ($R_V = 2.91$) to obtain individual extinctions for all the new confirmed massive OB type stars
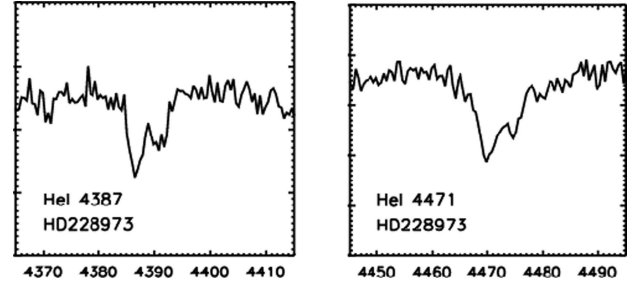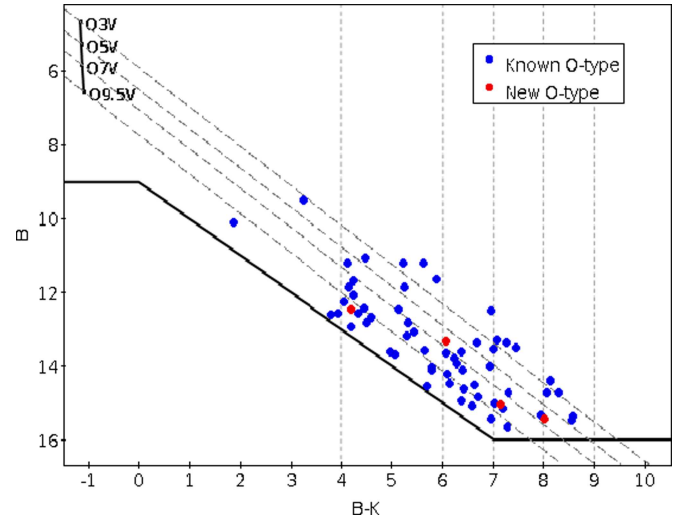
(see Table A.1). Most of them have visual extinctions in the range $A_V = 4-8$ mag, which agrees with previous studies in the region (Comerón & Pasquali 2012; Wright et al. 2015). But, as in Comerón & Pasquali (2012), this is partly consequence of the imposed $B \leq 16$ and $Ks < 9$ magnitude limits.

In Fig. 3 we present the B, $(B - K)$ diagram of the confirmed O-type stars in Cygnus OB2. We observe that some of them are aligned below the O9.5V reddening vector, which could suggest a small shift in the adopted intrinsic color calibration since most of them are already known dwarf late O-type members. In spite of this we can assess the incompleteness of the O population in the region by taking into account the ratios of stars in different spectral (O3-O5, O5-O7 and O7-O9.5) and $(B - K)$ color bins.

All the stars of our sample with $(B - K)$ colors <6 mag should be bright enough to have been detected by our selection criteria. Figure 3 shows that the population is expected to be complete for $(B - K) < 7$ mag. But for $(B - K) > 7$ mag we can not see late O-type stars because they are fainter than $B = 16$ mag, which is the imposed magnitude limit. Assuming that the ratios of spectral types are independent of extinction, we can conclude we are loosing the fainter or more obscured O-type stars.
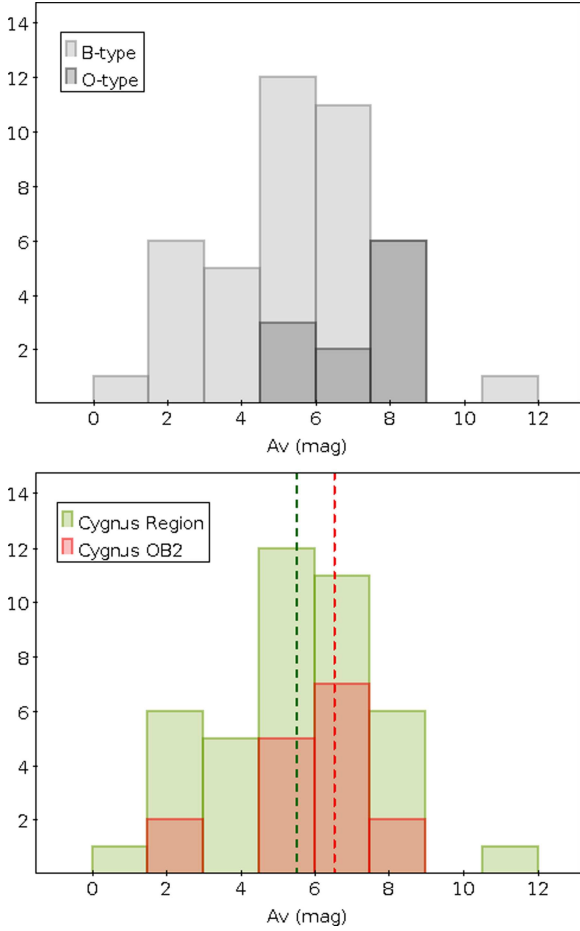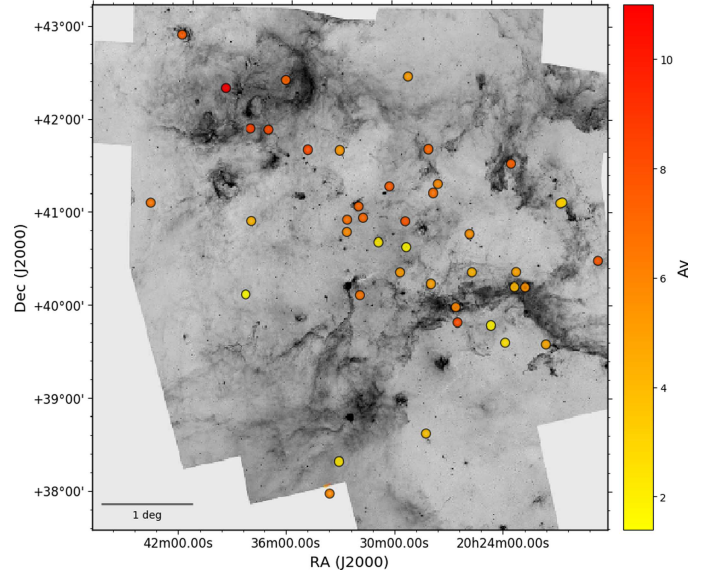
Fig. 5. Location of the new confirmed OB stars in the region colored according to the derived extinction (A_V) and over-plotted on an inverse *Spitzer* 8 μm image.

a very bright star. These cases show again that the sample does not provide a complete census. The magnitude-limited sample of Cygnus OB2 is made incomplete due to extinction.

In Fig. 5 we present the spatial location of the new classified OB stars, where each star is color-coded according to its derived visual extinction A_V. The extinction distribution varies smoothly across the region, increasing from the south-west (Cygnus OB9) to the northeast (Cygnus X-North) where the most extinguished star of our sample, J20395358+4222506, is located.

4.2. Stellar parameters

4.2.1. Effective temperature

For each classified O-type star and luminosity classes V, III and I, we have used the effective temperature (T_{eff}) scale developed by Holgado et al. (in prep.) based on a revision of the O-type standards in the IACOB database. We have preferred it over the SpT-T_{eff} calibration suggested by Martins et al. (2005) since the latter gives too low T_{eff} values for late O-type stars (Simón-Díaz et al. 2014).

For early B-type stars and luminosity class V, we decided to use the T_{eff} spectral type compilation of Nieva (2013). An excellent agreement with the calibration of Holgado et al. is found. For late B-type dwarf stars we have used the calibration of Pecaut & Mamajek (2013). Regarding B stars with luminosity class I, we have used the T_{eff} scale of Markova & Puls (2008), and for luminosity class III we have interpolated between classes I and V. In Fig. 6 are represented the different T_{eff} scales adopted in this work, and the derived T_{eff} values for all the new OB type stars are shown in Table A.1. We see that all scales for B-types fit smoothly the Holgado et al. scale. Temperatures were also obtained for those stars classified as SB2 binaries by taking into account the primary component.

Comerón & Pasquali (2012) used the "observational" effective temperature based on the T_{eff} versus spectral type calibration of Martins et al. (2005). For B-type stars, they used the T_{eff} spectral type compilation of Tokunaga (2000) but applying a scaling factor to force the agreement with Martins et al. (2005) temperature scale. In order to be consistent with them we have
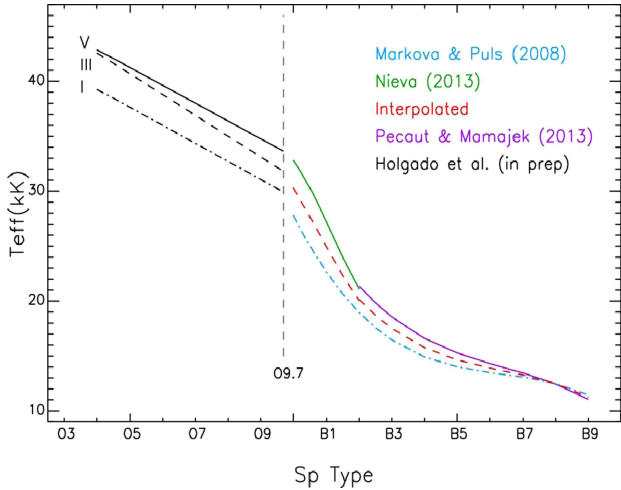
Fig. 4. *Top*: extinction distribution of the new classified OB type stars earlier than B3 in Cygnus OB2 and boundaries. Gray indicates B-type stars while dark gray are O-type stars. *Bottom*: green indicates all the confirmed stars in the Cygnus region, which includes Cyg OB2, Cyg OB9 and field. Red indicates only those new OB stars located in Cygnus OB2. Green and red dashed lines indicate the median values for the stars in the whole Cygnus region and only Cygnus OB2 respectively.

The extinction distribution for the 42 new confirmed OB stars earlier than B3 in Cygnus OB2 and boundaries is shown in Fig. 4 (top). Again, the spectral classification for those stars classified as possible or confirmed SB2 binaries is taken from the primary component. Although O-type stars are clearly more obscured, a median value of A_V = 5.5 mag was found for the whole sample. However, this value is also affected by completeness. O-type stars are more obscured on average because we can detect them up to higher foreground extinctions thanks to their intrinsic brightness. In the bottom histogram the same sample is differentiated by location: the whole sample that belongs to Cygnus OB2, Cygnus OB9 and boundaries, and as a sub-sample, those stars located within the Cygnus OB2 area (from Comerón & Pasquali 2012) for which a median value of A_V = 6.5 mag is derived.

We see an abrupt cut for $A_V \geq 9$ mag. Stars with such high visual extinctions shall be intrinsically extremely bright to be seen. An O9V star with a visual extinction of A_V = 9 mag will have an apparent magnitude $B \simeq 17$ mag, beyond the selection criteria limits and probably this is the reason why we do not find stars beyond this value. However, for the star J20395358+4222506 classified as B0I, we have obtained a visual extinction of 11.0 mag. It has a magnitude in the B band of 15.89 mag but in the Ks band of only 5.82 mag which indicates

Fig. 6. T_{eff} scales used in this work.

recalculated temperatures for all of their known OB stars sample in the Cygnus Region using our criteria. New values are shown in Table A.2.

4.2.2. Bolometric correction and luminosity

As Comerón & Pasquali (2012), we have adopted a distance modulus of $DM = 10.8$ mag, and used the intrinsic magnitudes derived by Martins & Plez (2006) for O stars and those compiled by Tokunaga (2000) for B stars. Thus we could derive absolute magnitudes (see Comerón et al. 2008). To derive luminosities we adopted bolometric corrections (BCs) from Lanz & Hubeny (2003, 2007). There is an excellent agreement with Martins et al. (2005) for temperatures higher than ~32 000 K, and also with the bolometric corrections from Nieva (2013) for cooler stars (see Nieva 2013). The derived luminosity values for the new and already known OB stars are shown in Table A.1 and Table A.2, respectively.

5. Discussion

Some of the new confirmed OB type stars (see Fig. 1) are located at the boundaries assigned to Cygnus OB2. However, the limits of the association are not strongly defined. The first surveys in the association assumed a smaller area where the most luminous members are located (Münch & Morgan 1953; Massey & Thompson 1991). Then, Knödlseder (2000) provided wider limits showing that extinction was a limiting factor in previous studies. This area was thus extended with the identification of new early-type members (Comerón et al. 2002, 2008; Comerón & Pasquali 2012; Wright et al. 2009; Wright et al. 2015). If we assume the extension of Cygnus OB2 as the area adopted by Comerón & Pasquali (2012) (1 deg. radius centered on Galactic coordinates $l = 79.8°$ and $b = +0.8°$), as well as the most recent census in the area developed by Wright et al. (2015), we can now update the census of O and B-type stars in Cygnus OB2 from 204 to 221, and the number of confirmed O-type members increases from 66 to 70 stars.

5.1. Hertzsprung-Russell diagram

Some studies about the age of Cygnus OB2 have been developed in the last two decades (Massey et al. 2001; Hanson 2003; Drew et al. 2008; Negueruela et al. 2008; Wright et al. 2010;

Comerón & Pasquali 2012; Comerón et al. 2016). However, different evolutionary stellar models were used. We decided to explore four different stellar models (two families with two initial rotational velocities) to construct the HRD in order to assess uncertainties on the age distribution.

We have placed the new confirmed OB stars in the HRD to study the evolutionary status of the association. For this aim we have considered the stars within the area adopted by Comerón & Pasquali (2012). We have also added the already known OB stars compiled in their work to complete the sample. Two of them, classified as B0 stars (J20325964+4115146 and J20333700+4116113) were recently reclassified as O9.7III and O9.5IV by Maíz Apellániz et al. (2016). We thus decided to assume this last classification for both. We have used the Geneva evolutionary tracks and isochrones with and without rotation as calculated by Ekström et al. (2012) (Fig. 7, top), and for comparison, the Bonn evolutionary tracks and isochrones with and without rotation as calculated by Brott et al. (2011) (Fig. 7, bottom).

In the Geneva case, we found a difference up to ~2 Myr in the stellar ages for those most massive members (≥ 20 $M_\odot$) depending on whether we consider rotation or not. Larger stellar lifetimes are derived from rotating stellar models. A similar result was found by Wright et al. (2015) by comparing both non-rotating and rotating Geneva stellar models. They derived an age range of 1–7 Myr for the association, but the results from rotating stellar models suggested an age of 4–5 Myr, while non-rotating models hinted at a younger age (~2–3 Myr). On the contrary, the Bonn stellar models included on this work do not exhibit a large difference in the estimated age of the stars when they include or not stellar rotation. This different behavior is most likely to be ascribed to their different treatment of rotation. Thus, the positions of the isochrones in both Bonn HR diagrams are very similar. Moreover, in the Bonn case we see an extended terminal age main sequence (TAMS), and therefore, all the OB stars are located on the main sequence (MS). In spite of this, all models suggest that most of the stars are in the age range of 1–6 Myr, indicating a continuous (but not necessarily constant) star formation activity. However, a combination of different scenarios (rotating and non-rotating stellar models) would help to narrow the possible ages. Slow rotators with initial masses of 30 $M_\odot$ or less would give similar ages as more massive stars born with larger rotational velocities.

In view of the results, we can conclude that uncertainties due to rotation and adopted models affect mainly the most massive members, suggesting larger ages of about 1–2 Myr for them. This makes the age determination very uncertain and strengthens the need for additional diagnostics, in particular individual rotation velocity measurements, to better constrain them.

5.2. Age distribution across Galactic longitude

Comerón & Pasquali (2012) studied the correlation between ages and Galactic longitudes in Cygnus OB2. They suggest that star formation has proceeded from lower to higher Galactic longitudes, finding most of the old stars located at low Galactic longitudes while the youngest ones lie at higher Galactic longitudes. In order to corroborate it, we have obtained ages by comparing isochrones from the HRDs, and divided the sample of OB stars in three age groups: the young group contains stars in the range of 0–5 Myr, the intermediate group contains stars in the range of 5–10 Myr, and the old one contains stars with ages >10 Myr.
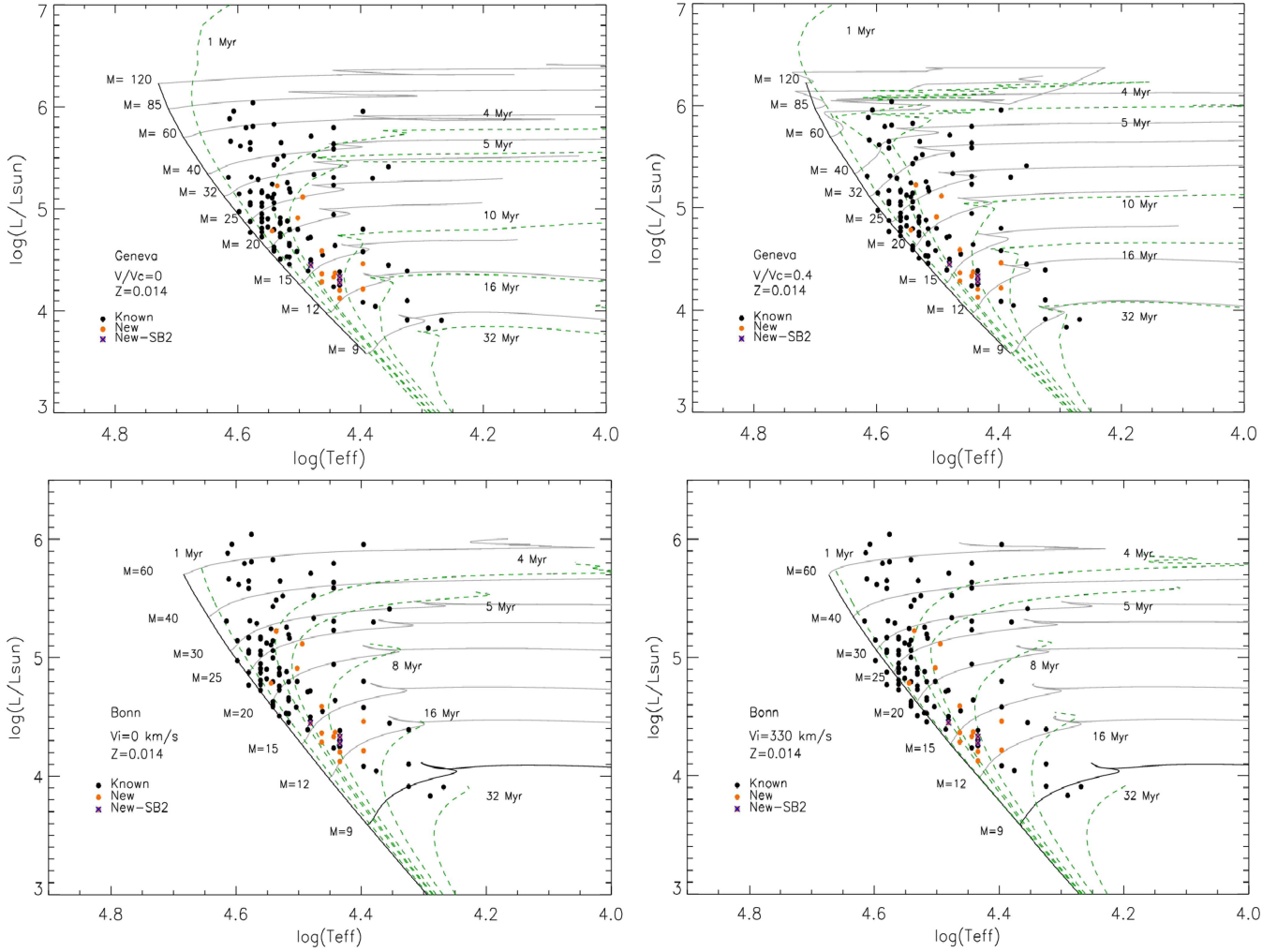
Fig. 7. HR diagrams of OB stars in Cygnus OB2 assuming a *DM* = 10.8 mag. Known OB stars from Comerón & Pasquali (2012) are also included to complete the sample. Black and orange dots indicate the already known and new OB-type stars respectively. Blue crosses indicate those new stars classified as possible SB2 stars. *Top left hand panel*: isochrones (dotted lines) and evolutionary stellar tracks (solid lines) for non-rotating models from Ekström et al. (2012). *Top right hand panel*: isochrones (dotted lines) and evolutionary stellar tracks (solid lines) for rotating models (V/V$_c$ = 0.4) from Ekström et al. (2012) . *Bottom left hand panel*: isochrones (dotted lines) and evolutionary stellar tracks (solid lines) for non-rotating models from Brott et al. (2011). *Bottom right hand panel*: isochrones (dotted lines) and evolutionary stellar tracks (solid lines) for rotating models (V$_i$ = 330 km s^{-1}) from Brott et al. (2011).

Figures 8 and 9 show the histograms of the relative frequency of our OB type sample located at low (78.5°–79.5°), central (79.5°–80.5°) and high (80.5°–81.5°) Galactic longitudes in each age group and for each model considered (Geneva (Fig. 8) and Bonn (Fig. 9) rotating and non-rotating models). In all cases, most of the stars at high Galactic longitudes belong to the young-intermediate age group, while those stars located at low Galactic longitudes belong to the old age group. We only obtain significant age differences at using the rotating Geneva models since in this case rotation gives older ages for the most massive stars. Thus, we can see a change in the relative frequencies of old and intermediate stars. On the other hand, we do not see these age differences at using rotating Bonn models because of their lower sensitivity to rotation as noted earlier.

This analysis thus supports the correlation between ages and Galactic longitudes in Cygnus OB2 as previously suggested by Comerón & Pasquali (2012). Massive star formation in Cygnus OB2 seems to have proceeded from lower to higher Galactic longitudes, regardless of the details of the models used.

5.3. The whole Cygnus region

In order to obtain a big picture of the age distribution across the Galactic longitude, we have performed the same analysis as in Cygnus OB2 but now in a wider area which includes Cygnus OB2, Cygnus OB9 and boundaries. We have placed the whole sample of OB stars, including late B-type stars, in an HRD (see Fig. 10). Due to the similar results obtained in Cygnus OB2 by using different models, we have now used isochrones and evolutionary stellar tracks for non-rotating models from Ekström et al. (2012). We derived ages by comparison with isochrones and divided again the sample in three age groups: the young group (0–5 Myr), the intermediate group (5–10 Myr), and the old group (>10 Myr). In Fig. 11 we show the spatial distribution of the different age groups, where most of the younger stars (left) are concentrated at higher Galactic longitudes, while the older ones (right) are located at central-lower Galactic longitudes. These results suggest that massive star formation has proceeded from lower to higher Galactic longitudes,
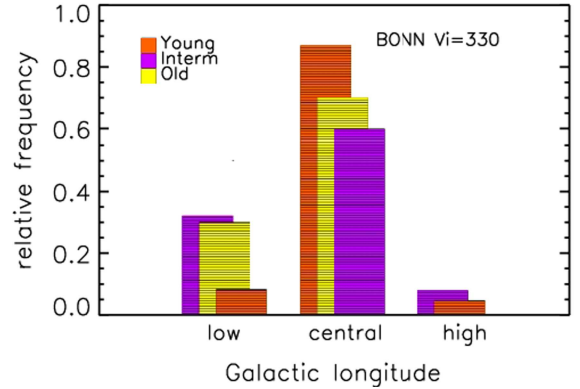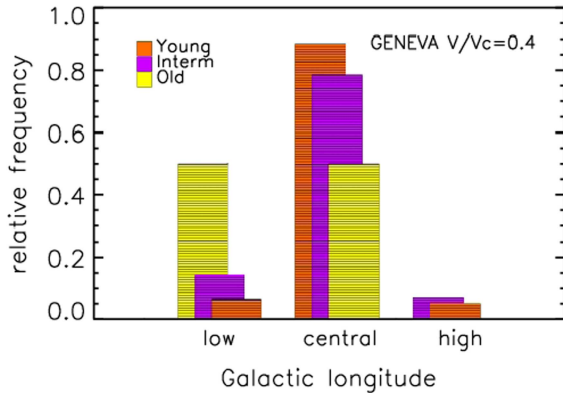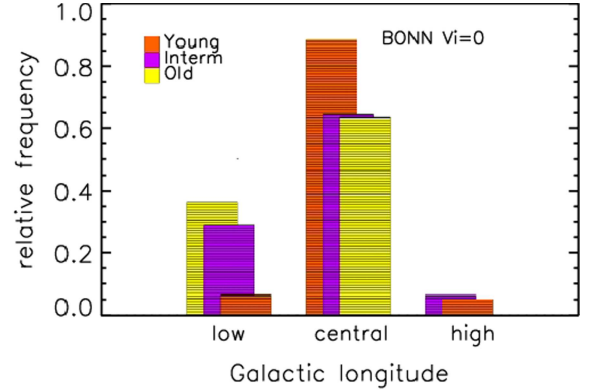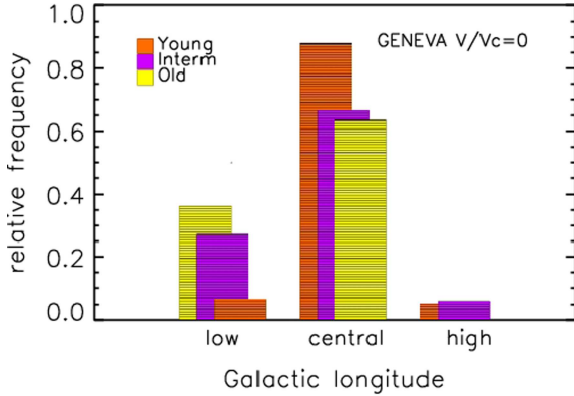
Fig. 8. Relative frequency histograms of the stars located at low (78.5°–79.5°), central (79.5°–80.5°) and high (80.5°–81.5°) Galactic longitudes in Cygnus OB2 using Geneva non-rotating (*top*) and rotating (*bottom*) models. Orange, purple and yellow colors indicate those stars located in the young (0–5 Myr), intermediate (5–10 Myr) and old (>10 Myr) age groups.

Fig. 9. Relative frequency histograms of the stars located at low (78.5°–79.5°), central (79.5°–80.5°) and high (80.5°–81.5°) Galactic longitudes in Cygnus OB2 using Bonn non-rotating (*top*) and rotating (*bottom*) models. Orange, purple and yellow colors indicate those stars located in the young (0–5 Myr), intermediate (5–10 Myr) and old (>10 Myr) age groups.

from Cygnus OB9 to Cygnus OB2, with a strong peak in the northern part of the association.

6. Conclusions

We have carried out several observing runs between 2013 and 2017 to obtain new blue intermediate-resolution spectra suitable for spectral classification for the magnitude-limited ($B \leq 16$ mag, $Ks < 9$ mag) candidate list compiled by Comerón & Pasquali (2012). Out of 61 candidates, we confirm 42 new massive OB-type stars, earlier than B3, including 11 new O-type members. A 21% of this sample results on confirmed or possible SB2 binaries. Two other stars are late-B, seven are A-type, six are F-type, and the remaining four are G-type stars. Therefore, the spectral classification of the homogeneously selected sample is now completed. The selection criteria success rate obtained by Comerón & Pasquali (2012) along with this work is 72%, supporting the success at identifying reddened massive OB stars with the reddening-free parameters based on *BJHK* photometry (see Sect. 2). However, the magnitude cutoff and dust extinction introduce an incompleteness. We loose the faintest and more obscured late O-type members in Cygnus OB2, and we are still far to obtain a complete census of the early-type population in the association.

We have also estimated individual visual extinctions (A_V) for the new confirmed OB-type stars using the extinction law derived by Wright et al. (2015). We found a median value of ~5.5 mag for the stars in the whole Cygnus region, and as we

expect, a large median value of ~6.5 mag for those stars within the Cygnus OB2 association.

We have placed the new sample of OB stars in the HR diagram using both rotating and non-rotating models calculated by Ekström et al. (2012) and Brott et al. (2011) in order to assess uncertainties. We have also placed the already known OB type stars compiled by Comerón & Pasquali (2012) for completeness. To this aim, we derived effective temperatures and luminosities using spectral type calibrations for the whole sample. Although coming from different sources, our adopted calibrations fit very well with each other. Uncertainties about rotation and adopted models affect only the most massive members, suggesting larger ages for them of ~1–2 Myr. Even so, all models support the previous age spread observed in Cygnus OB2 of ~1–6 Myr.

In order to check the correlation between age and Galactic longitude found by Comerón & Pasquali (2012) in Cygnus OB2, we have divided the sample of OB stars in different location and age groups by comparing with isochrones: the young group (0–5 Myr), the intermediate group (5–10 Myr), and the old group (>10 Myr). Despite the differences in physical process treatment (rotation and physics of the stellar interior) done by the Geneva and Bonn groups, the spatial distribution of each age group is globally similar. Therefore, the result obtained by Comerón & Pasquali (2012) can not be an effect of using the Geneva stellar models without rotation when age dating the Cygnus region stars. Most of the stars at high Galactic longitudes belong to the young-intermediate age group, while stars at low Galactic longitudes belong to the old group. Assuming a wider area which includes Cygnus OB2, part of Cygnus OB9 and boundaries, we
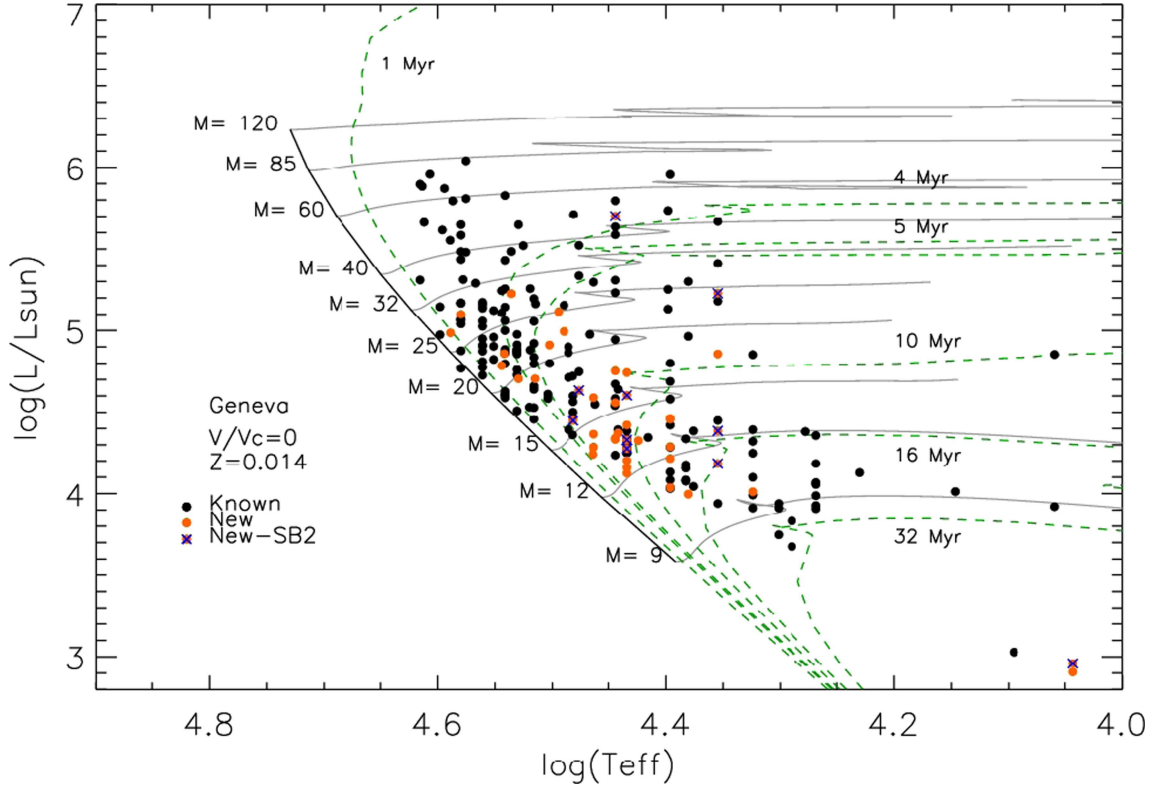
Fig. 10. HR diagram of OB stars in the Cygnus region (Cygnus OB2, Cygnus OB9 and field population) assuming a *DM* = 10.8 mag. Known OB stars from Comerón & Pasquali (2012) are also included to complete the sample. Black and orange dots indicate the already known and new OB-type stars respectively. Blue crosses indicate those new stars classified as possible or confirmed SB2 stars. Isochrones (dotted lines) and evolutionary stellar tracks (solid lines) for non-rotating models are from Ekström et al. (2012). Late-B stars are also included.
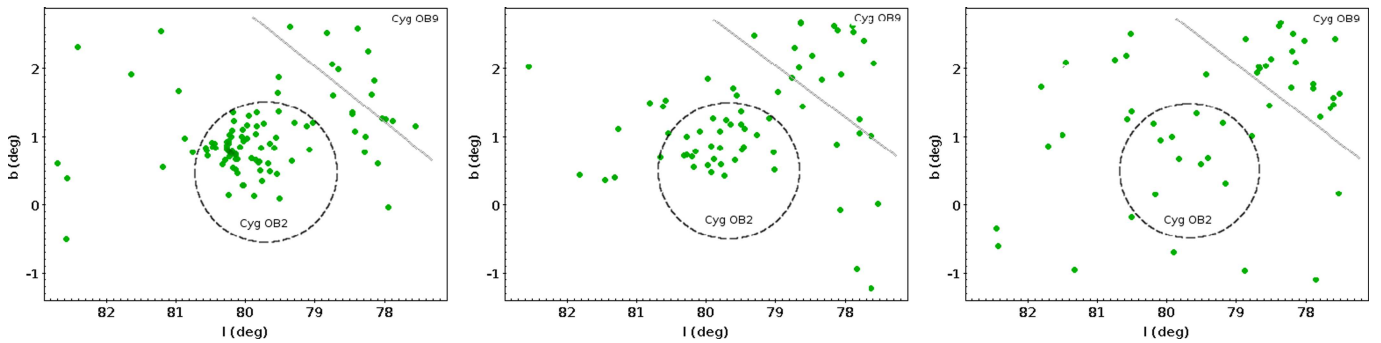

Fig. 11. Spatial distribution of stars of different age in the Cygnus area: the young population (0–5 Myr) on the *left*, the intermediate age one (5–10 Myr) in the *middle*, and the old population (>10 Myr) on the *right*.

obtain similar results suggesting that massive star formation in the region proceeds from Cygnus OB9 to Cygnus OB2, with a strong peak in the northern part of the association. Therefore the correlation between age and Galactic longitude is confirmed, regardless of the details of the models used.

References

Brott, I., de Mink, S. E., Cantiello, M., et al. 2011, A&A, 530, A115
Comerón, F., & Pasquali, A. 2012, A&A, 543, A101
Comerón, F., Pasquali, A., Rodighiero, G., et al. 2002, A&A, 389, 874
Comerón, F., Pasquali, A., Figueras, F., & Torra, J. 2008, A&A, 486, 453
Comerón, F., Djupvik, A. A., Schneider, N., & Pasquali, A. 2016, A&A, 586, A46
Crowther, P. A., Lennon, D. J., & Walborn, N. R. 2006, A&A, 446, 279
Drew, J. E., Greimel, R., Irwin, M. J., & Sale, S. E. 2008, MNRAS, 386, 1761
Ekström, S., Georgy, C., Eggenberger, P., et al. 2012, A&A, 537, A146
Gray, R. O., & Corbally, C. J. 2009, Stellar Spectral Classification (Princeton University Press)
Hanson, M. M. 2003, ApJ, 597, 957
Herrero, A., Corral, L. J., Villamariz, M. R., & Martín, E. L. 1999, A&A, 348, 542

Herrero, A., Puls, J., Corral, L. J., Kudritzki, R. P., & Villamariz, M. R. 2001, A&A, 366, 623

Herrero, A., Puls, J., & Najarro, F. 2002, A&A, 396, 949

Humphreys, R. M., & McElroy, D. B. 1984, ApJ, 284, 565

Kiminki, D. C., Kobulnicky, H. A., Kinemuchi, K., et al. 2007, ApJ, 664, 1102

Knödlseder, J. 2000, A&A, 360, 539

Lanz, T., & Hubeny, I. 2003, ApJS, 146, 417

Lanz, T., & Hubeny, I. 2007, ApJS, 169, 83

Lejeune, T., & Schaerer, D. 2001, A&A, 366, 538

Maíz Apellániz, J., Pellerin, A., Barbá, R. H., et al. 2012, in Proc. Scientific Meeting in Honor of Anthony, ed. F. J. Moffat, 465, 484

Maíz Apellániz, J., Sota, A., Arias, J. I., et al. 2016, ApJS, 224, 4

Markova, N., & Puls, J. 2008, A&A, 478, 823

Martins, F., & Plez, B. 2006, A&A, 457, 637

Martins, F., Schaerer, D., & Hillier, D. J. 2005, A&A, 436, 1049

Massey, P., & Thompson, A. B. 1991, AJ, 101, 1408

Massey, P., Johnson, K. E., & Degioia-Eastwood, K. 1995, ApJ, 454, 151

Massey, P., DeGioia-Eastwood, K., & Waterhouse, E. 2001, AJ, 121, 1050

Morgan, W. W., Johnson, H. L., & Roman, N. G. 1954, PASP, 66, 85

Münch, L., & Morgan, W. W. 1953, ApJ, 118, 161

Negueruela, I., Marco, A., Herrero, A., & Clark, J. S. 2008, A&A, 487, 575

Nieva, M.-F. 2013, A&A, 550, A26

Pecaut, M. J., & Mamajek, E. E. 2013, ApJS, 208, 9

Portegies Zwart, S. F., McMillan, S. L. W., & Gieles, M. 2010, ARA&A, 48, 431

Reddish, V. C. 1968, The Observatory, 88, 139

Reipurth, B., & Schneider, N. 2008, in Handbook of Star Forming Regions (ASP Monograph Publications), 4, 36

Rieke, G. H., & Lebofsky, M. J. 1985, ApJ, 288, 618

Rygl, K. L. J., Brunthaler, A., Sanna, A., et al. 2012, A&A, 539, A79

Sana, H., & Evans, C. J. 2011, Active OB Stars: Structure, Evolution, Mass Loss, and Critical Limits, IAU Symp., 272, 474

Schneider, N., Bontemps, S., Simon, R., et al. 2006, A&A, 458, 855

Schulte, D. H. 1956, ApJ, 124, 530

Schulte, D. H. 1958, ApJ, 128, 41

Simón-Díaz, S., & Herrero, A. 2007, A&A, 468, 1063

Simón-Díaz, S., Herrero, A., Sabín-Sanjulián, C., et al. 2014, A&A, 570, L6

Simón-Díaz, S., Negueruela, I., Maíz Apellániz, J., et al. 2015, Highlights of Spanish Astrophysics VIII, 576

Skrutskie, M. F., Cutri, R. M., Stiening, R., et al. 2006, AJ, 131, 1163

Sota, A., Maíz Apellániz, J., Walborn, N. R., et al. 2011, ApJS, 193, 24

Tokunaga, A. T. 2000, Allen's Astrophysical Quantities, 143

Walborn, N. R. 1971, ApJS, 23, 257

Walborn, N. R. 1973, AJ, 78, 1067

Walborn, N. R., Howarth, I. D., Lennon, D. J., et al. 2002, AJ, 123, 2754

Wright, N. J., Drake, J. J., & Drew, J. E. 2009, AAS Meet. Abstr., 213, 605.10

Wright, N. J., Drake, J. J., Drew, J. E., & Vink, J. S. 2010, ApJ, 713, 871

Wright, N. J., Drew, J. E., & Mohr-Smith, M. 2015, MNRAS, 449, 741

Zacharias, N., Urban, S. E., Zacharias, M. I., et al. 2004, AJ, 127, 3043

Zacharias, N., Finch, C., Girard, T., et al. 2010, AJ, 139, 2184

Appendix A: Table of stellar parameters

Table A.1 shows the derived stellar parameters for the new classified OB stars in a large area which includes Cygnus OB2 and its surroundings. We have also included the derived individual visual extinctions. Table A.2 shows the updated temperatures and luminosities for the already known OB stars from Comerón & Pasquali (2012) assuming the same spectral calibrations used in this work (see Sect. 4.2).

Table A.1. Temperatures, luminosities, and individual visual extinctions derived for the new classified massive OB stars.

Object	SpT	$T_{\rm eff}$ (K)	$\log (L/L_\odot)$	$A_{\rm V}$ (mag)
Cygnus OB2				
J20345785+4143543	O7:Ib	34990	5.25	8.2
J20293563+4024315	O8IIIz	33961	4.75	5.1
J20275292+4144067	O9.5II	30626	5.09	7.1
J20291617+4057372	O9.7III	28518	4.78	7.7
J20273787+4115468	B0II	25932	4.62	6.8
J20301097+4120088	B0:II:	25932	4.39	7.4
J20323968+4050418	B0II	25932	4.32	5.7
J20323882+4058469	B0Ib	27800	4.33	6.7
J20272099+4121262	B0.5V	26308	4.33	5.8
J20330526+4143367	B0.5III	24164	4.27	5.2
BD+404208	B1V	23590	4.14	2.2
J20314341+4100021	B1V	23590	4.21	7.0
J20315898+4107314	B1V	23590	4.26	7.1
BD+404193	B1V	23590	4.06	1.7
J20274925+4017004	B1III	21557	4.27	4.9
J20315433+4010067	B1III	21557	4.02	6.5
CCDMJ20323+4152AB	B9V	10700	2.96	–0.2
Surroundings				
J20423509+4256364	O6IIIz	38192	4.97	7.4
J20371773+4156316	O7V	36872	5.06	8.2
J20222481+4013426	O8II	33570	4.69	5.5
J20261976+3951425	O8.5IV	33391	4.81	8.0
J20262484+4001413	O9.2III	31317	4.65	5.9
J20382173+4157069	O9.7II	30859	4.99	8.5
J20181090+4029063	O9.7Ib	28644	4.58	7.6
J20395358+4222506	B0I	25094	5.57	11.0
J20281176+3840227	B0Ib	25094	4.43	3.6
J20290247+4231159	B1Ib	19979	4.03	5.0
J20225451+4023314	B0Iab	25094	4.21	4.7
J20253320+4048444	B0Iab	25094	4.62	5.5
HDE229258	B0.7V	24949	4.13	1.8
J20361806+4228483	B0.7III	22860	4.14	7.2
J20233816+3938118	B0.7Ib	21514	3.87	2.3
HD 228973	B1V	23590	4.45	2.4
J20201435+4107155	B1V	23590	4.27	3.4
J20230290+4133466	B1V	23590	4.68	7.2
J20330453+3822269	B1V	23590	4.09	2.4
J20230183+4014029	B1III	21557	4.26	4.3
J20382889+4009566	B1III	21557	3.84	1.4
J20440752+4107342	B1III	21557	4.09	6.5
LSII+3797	B1Ia	19979	5.07	5.8
J20211924+3936230	B1Ib	19979	4.23	4.6
BD+394179	B1Ib	19979	4.70	4.2
J20381289+4057169	B2V	20549	3.98	4.2
BD+423785a	B9V	10700	2.90	0.6

Table A.2. Temperatures and luminosities derived for the known massive OB stars from Comerón & Pasquali (2012).

Object	RA (hhmmss)	Dec (° ′ ″)	SpT	T_{eff} (K)	$\log (L/L_\odot)$
Cygnus OB2					
J20331411+4120218	20:33:14.110	+41:20:21.91	O3If	40910	5.66
J20330879+4113179	20:33:08.818	+41:13:17.93	O4III	41070	5.88
J20360451+4056129	20:36:04.500	+40:56:13.01	O5V((f))	41250	5.31
J20331798+4118311	20:33:17.982	+41:18:31.19	O5III	39440	5.62
J20340850+4136592	20:34:08.514	+41:36:59.39	O5I	37630	5.80
J20331074+4115081	20:33:10.735	+41:15:08.22	O5If	37630	6.04
J20332346+4109130	20:33:23.471	+41:09:12.90	O5.5V	40440	5.96
J20331326+4113287	20:33:13.264	+41:13:28.67	O6V	39630	5.14
J20303980+4136506	20:30:39.805	+41:36:50.63	O6V	39630	4.97
J20344410+4051584	20:34:44.146	+40:51:58.67	O6.5III(f)	37845	5.31
J20283203+4049027	20:28:32.027	+40:49:02.88	O7	38010	5.65
J20310019+4049497	20:31:00.204	+40:49:49.70	O7V((f))	38010	5.06
J20341350+4135027	20:34:13.511	+41:35:02.86	O7V	38010	5.04
J20331748+4117093	20:33:17.483	+41:17:09.35	O7V	38010	5.17
J20334086+4130189	20:33:40.863	+41:30:18.95	O7V	38010	4.77
J20342959+4131455	20:34:29.599	+41:31:45.49	O7V	38010	5.58
J20315961+4114505	20:31:59.609	+41:14:50.45	O7V	38010	4.87
J20321383+4127120	20:32:13.822	+41:27:12.01	O7IIIf	36900	5.29
J20313690+4059092	20:31:36.911	+40:59:09.06	O7Ib(f)	34350	5.48
J20323154+4114082	20:32:31.531	+41:14:08.18	O7.5Ib-II(f)	33530	5.52
J20323857+4125137	20:32:38.571	+41:25:13.79	O8V(n)	36390	5.02
J20274361+4035435	20:27:43.616	+40:35:43.51	O8V:	36390	4.72
J20331369+4113057	20:33:13.688	+41:13:05.77	O8V	36390	4.87
J20324545+4125374	20:32:45.450	+41:25:37.57	O8V	36390	5.16
J20331803+4121366	20:33:18.035	+41:21:36.67	O8V	36390	4.90
J20323486+4056174	20:32:34.865	+40:56:17.35	O8V	36390	4.77
J20300788+4123504	20:30:07.877	+41:23:50.44	O8V	36390	4.91
J20330292+4117431	20:33:02.913	+41:17:43.16	O8V	36390	5.06
J20325002+4123446	20:32:50.016	+41:23:44.70	O8V	36390	4.95
J20325919+4124254	20:32:59.057	+41:24:24.79	O8V	36390	4.81
J20333030+4135578	20:33:30.316	+41:35:57.88	O8V	36390	5.17
J20342193+4117016	20:34:21.934	+41:17:01.66	O8III+O8III	35010	5.11
J20323843+4040445	20:32:38.441	+40:40:44.48	O8III	35010	5.24
J20330292+4047254	20:33:02.928	+40:47:25.29	O8II((f))	33860	5.65
J20314540+4118267	20:31:45.403	+41:18:26.73	O8I	32710	5.16
J30332557+4133269	20:33:25.569	+41:33:26.88	O8.5V	35580	5.12
J20331634+4119017	20:33:16.256	+41:19:00.16	O8.5V	35580	4.82
J20332674+4110595	20:33:26.756	+41:10:59.42	O8.5V	35580	4.90
J20313749+4113210	20:31:37.506	+41:13:20.99	O9:	34770	5.83
J20335842+4019411	20:33:58.417	+40:19:41.13	O9:	34770	5.43
J20321656+4125357	20:32:16.563	+41:25:35.67	O9V	34770	4.79
J20311833+4121216	20:31:18.329	+41:21:21.65	O9V	34770	5.06
J20340486+4105129	20:34:04.851	+41:05:11.76	O9V	34770	4.59
J20311055+4131535	20:31:10.543	+41:31:53.53	O9V	34770	5.14
J20332101+4117401	20:33:21.016	+41:17:40.11	O9V	34770	4.63
J20331571+4120172	20:33:15.685	+41:20:18.75	O9V	34770	4.60
J20301839+4053466	20:30:18.391	+40:53:46.56	O9V	34770	4.99
J20314965+4128265	20:31:49.658	+41:28:26.50	O9III	33120	4.53
J20345606+4038179	20:34:56.057	+40:38:17.92	O9.7Iab	29922	5.33
J20305772+4109575	20:30:57.727	+41:09:57.51	O9.5V	33960	4.85
J20340601+4108090	20:34:06.017	+41:08:09.13	O9.5V	33960	4.87
J20335952+4117354	20:33:59.527	+41:17:35.46	O9.5V	33960	4.91
J20341605+4102196	20:34:16.046	+41:02:19.59	O9.5V	33960	4.73
J20272428+4115458	20:27:24.282	+41:15:45.82	O9.5V	33960	4.51
J20293480+4120089	20:29:34.798	+41:20:08.93	O9.5V	33960	4.76
J20323033+4034332	20:32:30.310	+40:34:33.22	O9.5IV	33067	5.25
J20333700+4116113	20:33:36.994	+41:16:11.31	O9.5IV	33067	4.88
J20334610+4133010	20:33:46.112	+41:33:01.00	O9.5Ia	30250	5.71
J20325964+4115146	20:32:59.633	+41:15:14.66	O9.7III	31797	4.80
J20283039+4105290	20:28:30.385	+41:05:29.04	OC9.7Ia	29922	5.52

Table A.2. continued.

Object	RA (hhmmss)	Dec (° ′ ″)	SpT	$T_{\rm eff}$ (K)	log $(L/L_\odot)$
J20302730+4113253	20:30:27.300	+41:13:25.13	Ofpe	38612	5.79
J20281547+4038196	20:28:15.471	+40:38:19.81	B0V:	32816	4.79
J20323951+4052475	20:32:39.507	+40:52:47.46	B0:V:	32816	5.19
J20331050+4122224	20:33:10.502	+41:22:22.44	B0V	32816	4.45
J20305552+4109575	20:30:55.516	+40:54:54.03	B0V	32816	4.66
J20295701+4109538	20:29:57.010	+41:09:53.84	B0V	32816	4.64
J20305111+4120218	20:30:51.115	+41:20:21.78	B0V	32816	4.53
J20331130+4042337	20:33:11.300	+40:42:33.73	B0:III:	30308	4.72
J20333821+4041064	20:33:38.213	+40:41:06.35	B0Ia	27800	5.64
J20344471+4051465	20:34:44.716	+40:51:46.73	B0Ia	27800	5.59
J20323904+4100078	20:32:39.057	+41:00:07.78	B0Ia	27800	5.79
J20322774+4128522	20:32:27.738	+41:28:52.26	B0Ib	27800	4.24
J20345878+4136174	20:34:58.781	+41:36:17.35	B0Ib(n)sb	27800	5.31
J20333822+4053412	20:33:38.218	+40:53:41.19	B0Ib	27800	4.94
J20333910+4119258	20:33:39.102	+41:19:25.98	B0Iab	27800	5.23
J20323498+4052390	20:32:34.848	+40:52:39.46	B0.2V	31906	4.58
J20292449+4052599	20:29:24.485	+40:52:59.85	B0.2IV	30588	4.71
J20321568+4046170	20:32:15.679	+40:46:17.00	B0.2IV	30588	4.39
J20294666+4105083	20:29:46.672	+41:05:08.32	B0.5V(n)sb	30288	4.50
J20282772+4104018	20:28:27.723	+41:04:01.80	B0.5V	30288	4.47
J20314605+4043246	20:31:46.053	+40:43:24.61	B0.5IV	28969	4.55
J20331870+4059379	20:33:18.696	+40:59:37.92	B0.5IIIe	27651	4.64
J20303970+4108489	20:30:39.701	+41:08:48.80	B0.7Ib	24014	5.30
J20294060+4109585	20:29:40.601	+41:09:58.54	B1[e]	27173	4.27
J20313338+4122490	20:31:33.378	+41:22:49.02	B1V	27173	4.25
J20340435+4108078	20:34:04.349	+41:08:07.91	B1V	27173	4.27
J20303833+4010538	20:30:38.329	+40:10:53.84	B1V	27173	4.34
J20293473+4020381	20:29:34.728	+40:20:38.09	B1V	27173	4.38
J20273982+4040384	20:27:39.821	+40:40:38.35	B1V	27173	4.28
J20303297+4044024	20:30:32.965	+40:44:02.41	B1V	27173	4.31
J20310464+4030568	20:31:04.659	+40:30:56.93	B1III:e	24903	5.95
J20334783+4120415	20:33:47.831	+41:20:41.37	B1III	24903	4.80
J20281539+4044046	20:28:15.392	+40:44:04.57	B1III	24903	4.58
J20310700+4035537	20:31:07.003	+40:35:53.73	B1III	24903	4.08
J20314885+4038001	20:31:48.848	+40:38:00.05	B1II	23767	4.04
J20333078+4115226	20:33:30.791	+41:15:22.70	B1I	22632	5.41
J20312203+4131284	20:31:22.026	+41:31:28.40	B1Ib:	22632	4.45
J20322734+4055184	20:32:27.339	+40:55:18.25	B2V	21092	4.39
J20312210+4112029	20:31:22.101	+41:12:02.87	B2V	21092	4.10
J20354703+4053012	20:35:47.026	+40:53:01.17	B2V	21092	3.91
J20284657+4107069	20:28:46.566	+41:07:06.86	B2II	19482	3.83
J20320689+4117570	20:32:06.877	+41:17:56.97	B3V	18546	3.91
Cygnus OB9					
HD 229196	20:23:10.784	+40:52:29.85	O5	41250	5.89
J20223777+4140292	20:22:37.766	+41:40:29.23	O5If	37630	5.48
BD+394177	20:25:22.122	+40:13:01.09	O6.5	38820	5.55
HD 229250	20:24:11.733	+39:40:41.54	O7	38010	5.44
BD+394168	20:24:21.475	+39:46:03.90	O7	38010	5.48
HD 229202	20:23:22.840	+40:09:22.53	O8V:	36390	5.14
BD+404159	20:25:06.521	+40:35:49.78	O9V	34770	4.61
BD+404148	20:23:14.549	+40:45:19.07	O9.5:V	33960	4.88
J20194916+4052090	20:19:49.156	+40:52:08.99	O9.5V	33960	4.86
J20190610+4037004	20:19:06.102	+40:37:00.39	O9.7Iab	29922	4.74
HD 193945	20:21:25.823	+41:11:39.56	B0Vnn	32816	4.92
BD+384058	20:23:28.531	+39:20:59.05	B0V	32816	4.83
LSII+4032	20:25:28.893	+40:12:54.13	B0III	30308	4.36
J20243872+3930301	20:24:38.720	+39:30:30.10	B0I:	27800	4.58
J20183413+4025045	20:18:34.130	+40:25:04.47	B0.2IV	30588	4.86
NGC6910-14	20:23:07.575	+40:46:08.87	B0.5V	30288	4.56
J20240515+4046035	20:24:05.154	+40:46:03.51	B0.5V	30288	4.60

Table A.2. continued.

Object	RA (hhmmss)	Dec (° ′ ″)	SpT	T_{eff} (K)	log ($L/L_\odot$)
HD 194092	20:22:05.443	+40:59:08.17	B0.5III	27651	4.39
HD 228882	20:18:57.784	+40:42:18.52	B0.5Ia	25014	5.25
HD 228929	20:19:36.542	+39:54:41.80	B0.5Ib	25014	5.13
J20234624+3937078	20:23:46.238	+39:37:07.83	B0.7IV	27818	4.54
J20241767+3920326	20:24:17.666	+39:20:32.56	B1V	27173	4.25
J20214868+4043005	20:21:48.682	+40:43:00.45	B1V	27173	4.32
HD 228919	20:19:27.908	+40:27:42.09	B1IV	26038	4.34
J20233375+4045199	20:23:33.752	+40:45:19.93	B1III	24903	4.03
J20223944+3935420	20:22:39.442	+39:35:42.02	B1III	24903	4.42
J20220454+4042487	20:22:04.541	+40:42:48.73	B1III	24903	4.28
J20215593+4110129	20:21:55.930	+41:10:12.92	B1III	24903	4.03
J20220879+3958161	20:22:08.793	+39:58:16.07	B1II	23767	4.38
J20214410+4012529	20:21:44.103	+40:12:52.91	B1Ia	22632	5.18
J20215160+3959496	20:21:51.600	+39:59:49.61	B1Ib	22632	3.94
J20203933+4031176	20:20:39.334	+40:31:17.64	B1.5V	24132	4.08
J20204933+4033027	20:20:49.333	+40:33:02.73	B1.5V	24132	4.15
HD 228911	20:19:21.712	+40:53:16.46	B2	21092	4.25
HD 194194	20:22:44.760	+40:42:52.63	B2III	20019	3.91
J20211677+4023162	20:21:16.773	+40:23:16.19	B2III	20019	3.94
J20250591+4020124	20:25:05.912	+40:20:12.44	B2III	20019	3.75
HD 228928	20:19:32.709	+40:39:13.75	B2Ib:nn	18945	4.38
HD 228941	20:19:40.169	+40:53:19.19	B3	18546	3.98
BD+404146	20:23:10.464	+40:45:52.34	B3	18546	4.35
NGC6910-16	20:23:07.301	+40:46:55.25	B3	18546	4.05
J20215115+3934215	20:21:51.149	+39:37:51.47	B3V	18546	4.18
J20221729+3946035	20:22:17.286	+39:34:21.50	B5Ia	14012	4.01
HD 228821	20:18:04.930	+40:06:06.80	B8	12449	3.03
HD 193426	20:18:39.749	+40:13:36.89	B9Ia	11457	4.85
Boundaries					
BD+433654	20:33:36.079	+43:59:07.38	O4If	39270	5.87
LSII+3953	20:27:17.572	+39:44:32.60	O7V:	38010	5.07
BD+423760	20:28:40.812	+43:08:58.46	O8.5V	35580	4.96
BD+423835	20:42:06.863	+43:11:03.72	O9p...	34770	5.25
J20342894+4156171	20:34:28.941	+41:56:17.09	O9V	34770	4.86
J20462826+4223417	20:46:28.255	+42:23:41.74	O9V	34770	4.88
J20272553+3929246	20:27:25.529	+39:29:24.58	O9.5V	33960	4.88
J20325571+4307583	20:32:55.713	+43:07:58.26	O9.5V	33960	4.97
J20310838+4202422	20:31:08.376	+42:02:42.25	O9.7II	30859	5.15
HD 199021	20:52:53.207	+42:36:27.87	B0V	32816	5.05
J20382040+4156563	20:38:20.413	+41:56:56.51	B0II	29054	5.29
J20385918+4202395	20:38:59.181	+42:02:39.45	B0Ib	27800	4.67
J20294195+3859342	20:29:41.952	+38:59:34.16	B0.2V	31906	4.61
J20352227+4355305	20:35:22.266	+43:55:30.46	B0.2IV	30588	4.90
BD+413794	20:32:02.204	+42:12:26.15	B0.2III	29270	4.97
HD 194839	20:26:21.545	+41:22:45.65	B0.5Iae	25014	5.73
J20313693+4201218	20:31:36.921	+42:01:21.79	B0.7Ib	24014	4.96
J20301273+3904216	20:30:12.732	+39:04:21.59	B1V	27173	4.24
LSIII+4217	20:35:10.623	+42:20:22.83	B1III	24903	4.69
J20374323+4232334	20:37:43.232	+42:32:33.40	B1III	24903	4.13
J20314215+4225532	20:31:42.151	+42:25:53.26	B1Ib	22632	5.67
BD+373976	20:33:49.752	+38:17:00.06	B1.5Vn	24132	4.17
J20313853+4152585	20:31:38.532	+41:52:58.46	B1.5V	24132	4.07
J20312725+4304227	20:31:27.253	+43:04:22.67	B1.5V	24132	4.33
BD+394189	20:26:20.922	+39:40:10.06	B2p?e?	21092	4.85
BD+413762	20:28:15.212	+42:25:39.14	B2V	21092	4.32
J20452110+4223514	20:45:21.103	+42:23:51.37	B2V	21092	3.99
J20264025+4233221	20:26:40.251	+42:33:22.09	B2II	19482	3.67
HD 196489	20:36:24.259	+39:11:40.70	B3V	18546	3.92
J20462289+4212311	20:46:22.892	+42:12:31.07	B3V	18546	4.06
HD 194779	20:25:55.077	+41:20:11.73	B3II	16983	4.12
BD+384098	20:27:33.010	+38:46:19.62	B9Ib	11457	3.92

Appendix B: Candidate spectra

In Fig. B.1 are plotted the normalized spectra of the 61 OB can- didates from the list of Comerón & Pasquali (2012). The spectra have been corrected for the stellar radial velocities and diagnostic lines are also indicated.
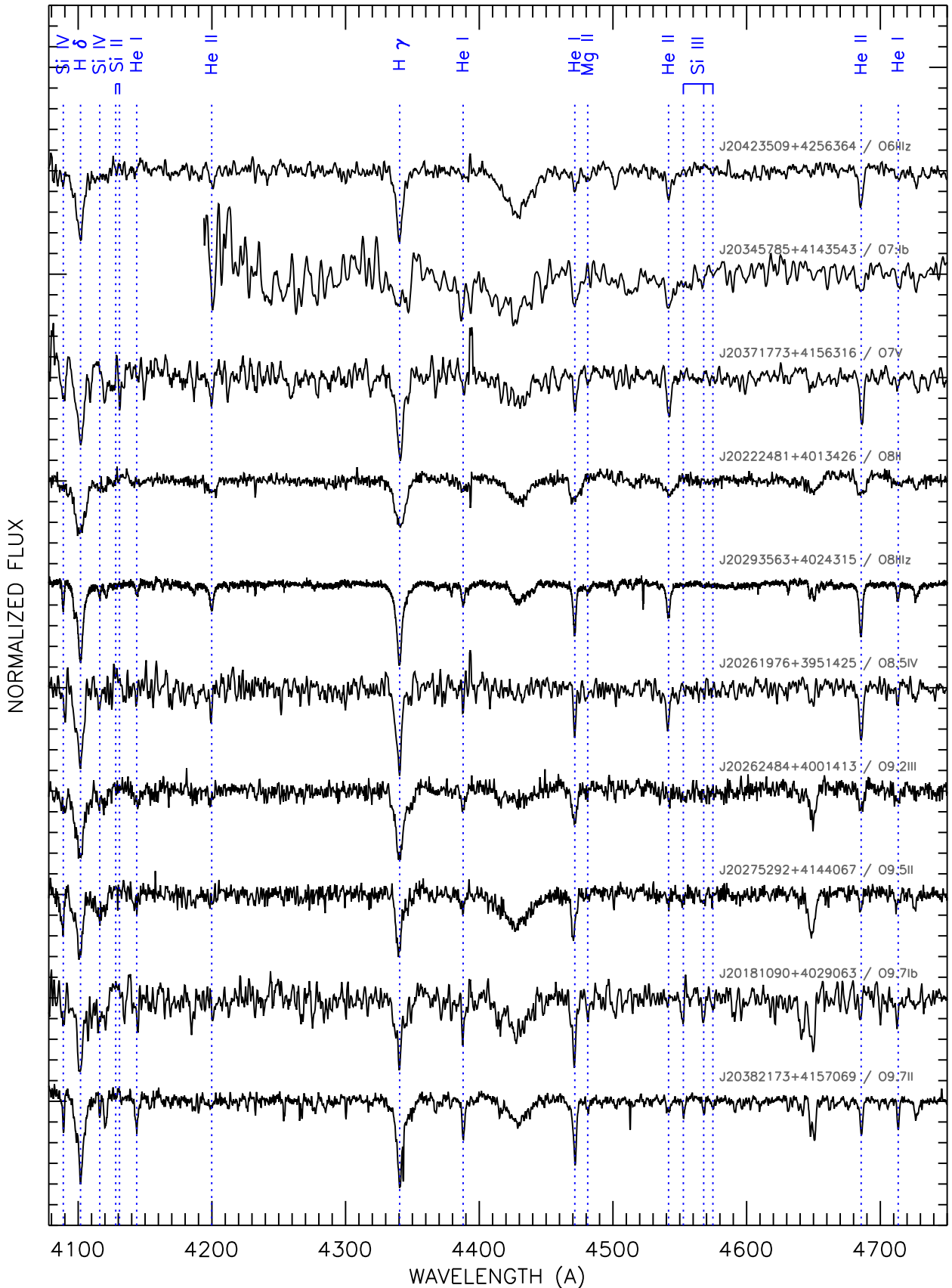

Fig. B.1. Spectra of the 61 OB candidate stars where dotted vertical lines indicate H, He, Si and Mg lines in the wavelength range.
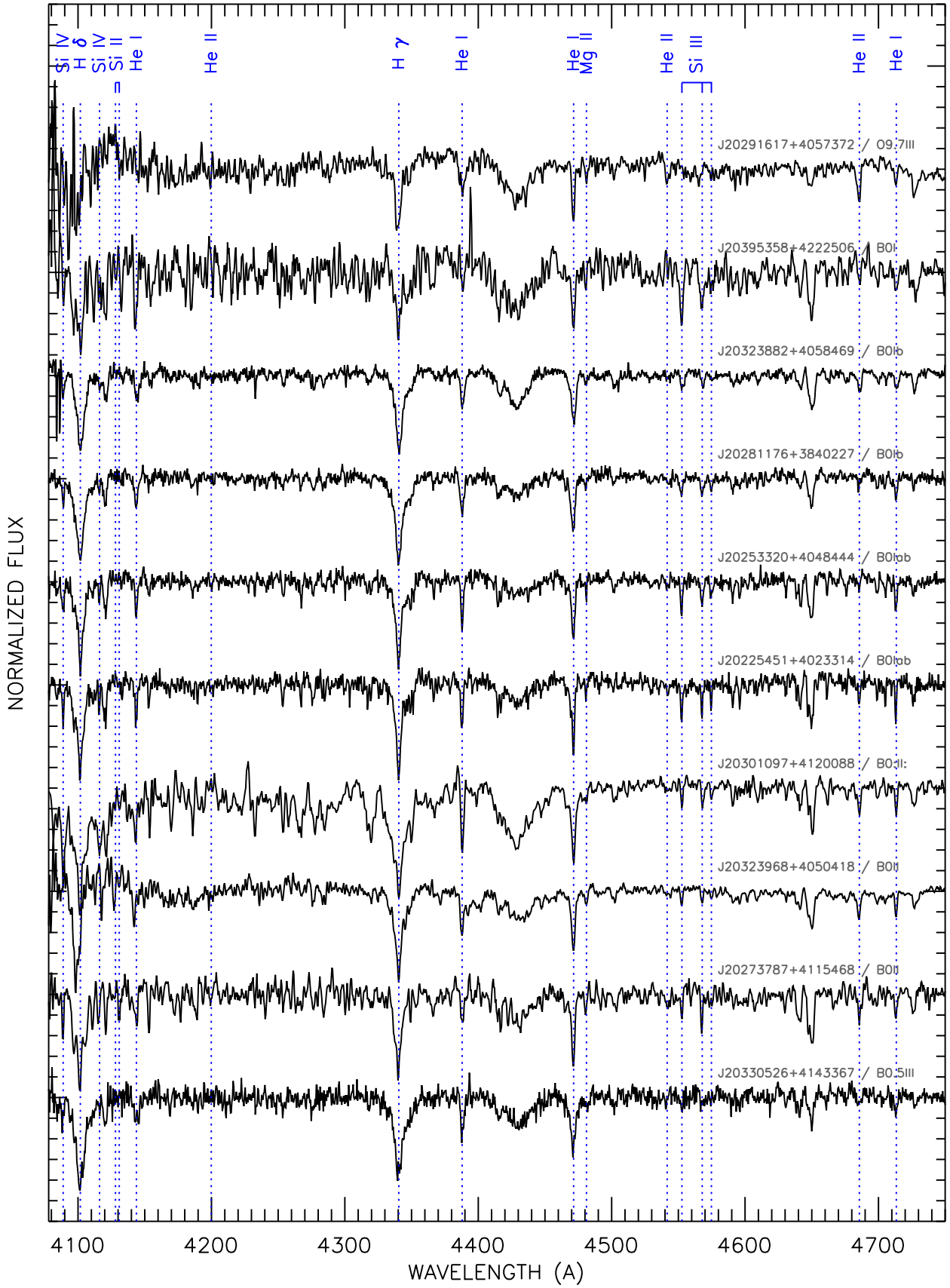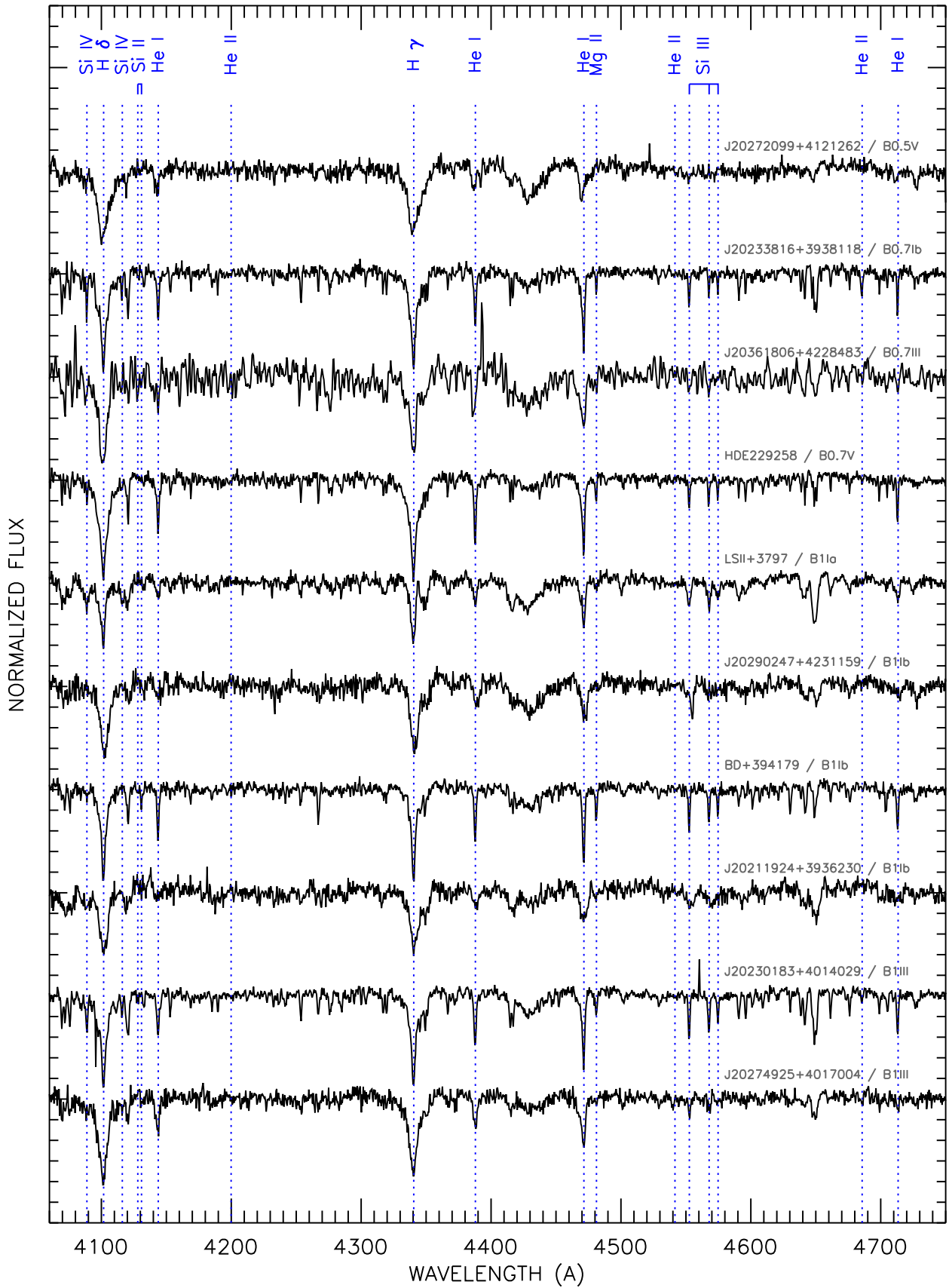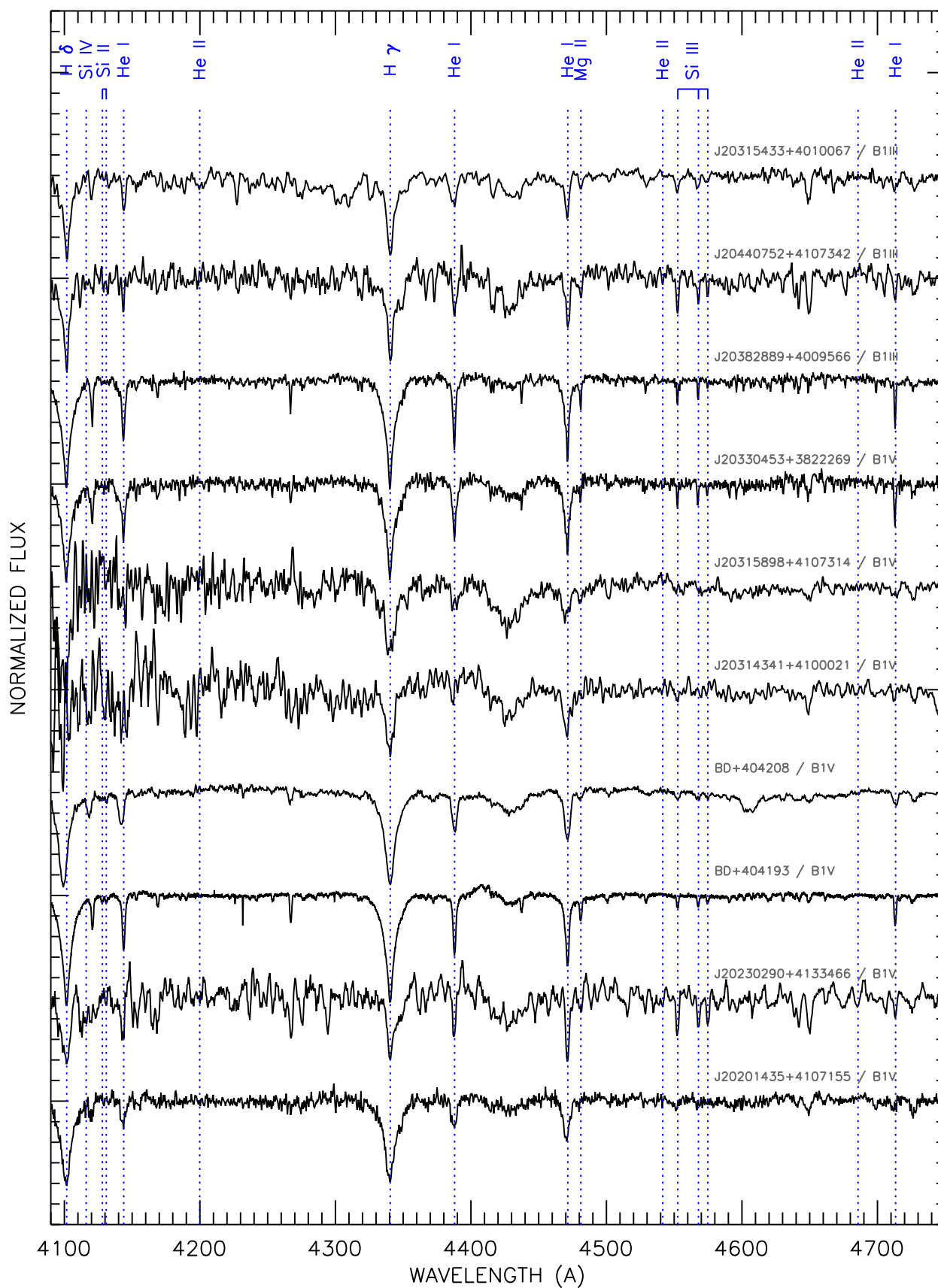
Fig. B.1. continued.

Fig. B.1. continued.

Fig. B.1. continued.
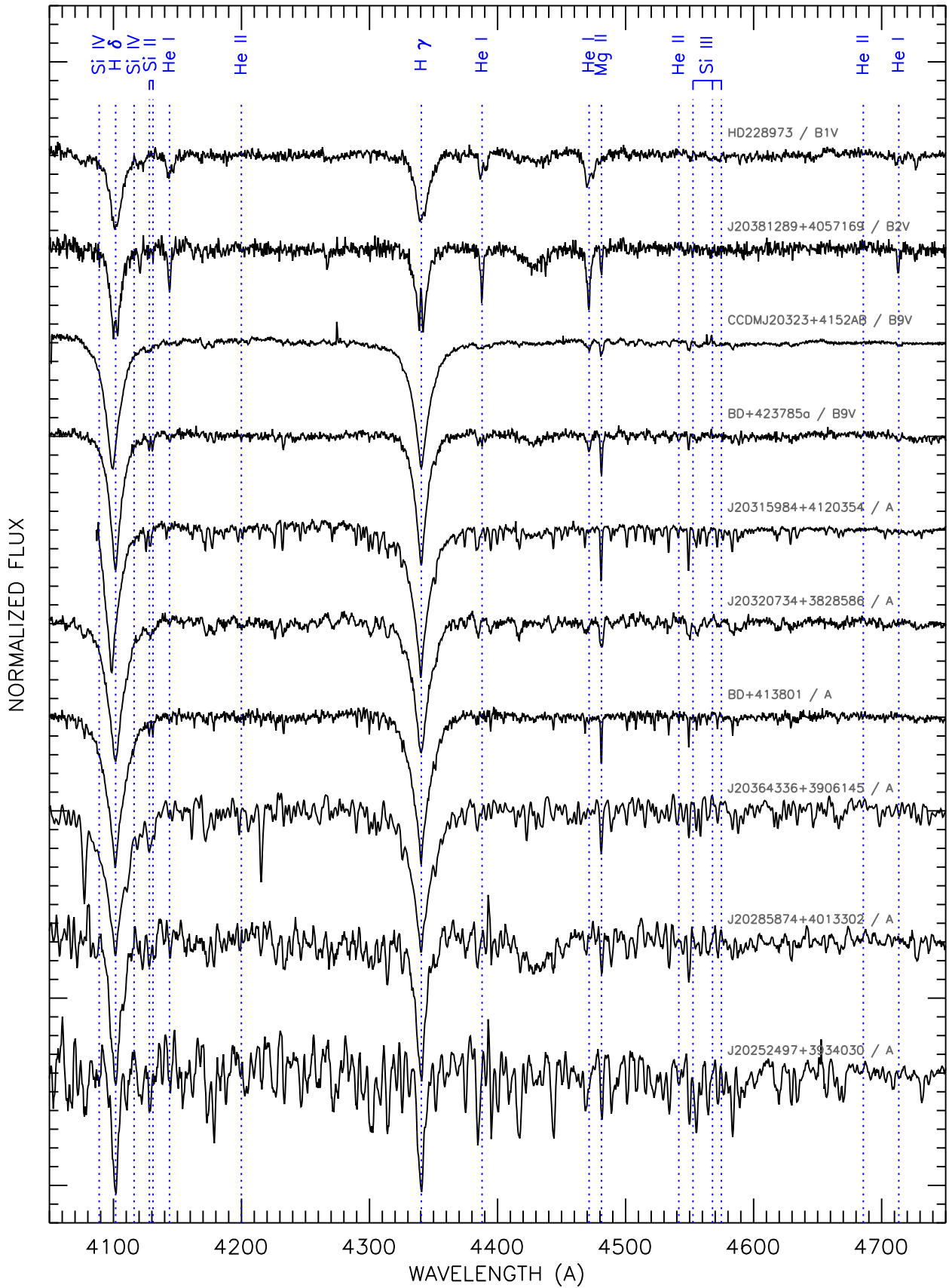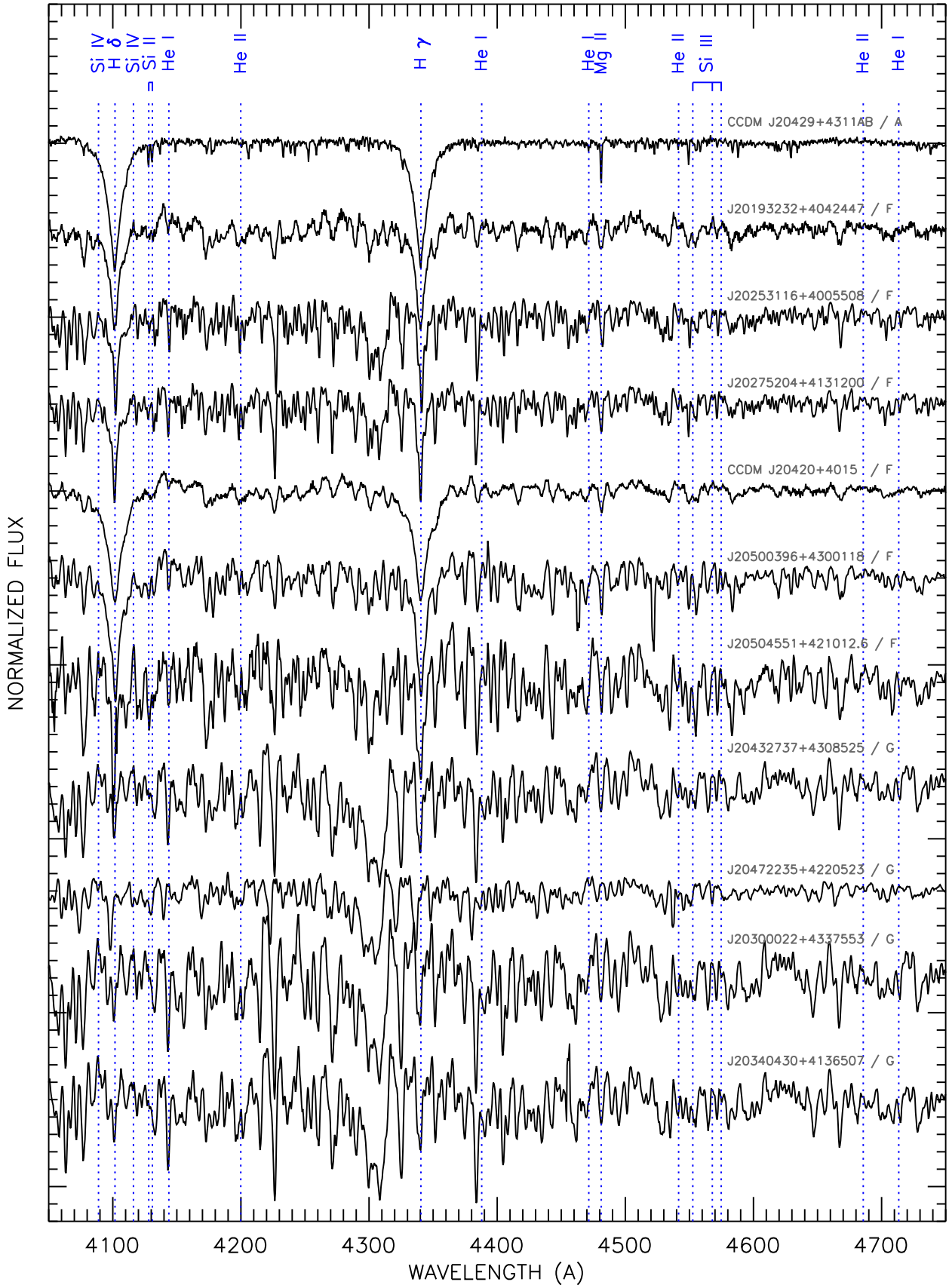
Fig. B.1. continued.

Fig. B.1. continued.